

Reaction mechanisms of $\text{Li}_{0.30}\text{La}_{0.57}\text{TiO}_3$ powder with ambient air: H^+/Li^+ exchange with water and Li_2CO_3 formation

Anthony Boulant,^a Jean Francois Bardeau,^a Alain Jouanneaux,^a Joël Emery,^a Jean-Yves Buzare^a and Odile Bohnke^{*b}

Received 24th November 2009, Accepted 15th February 2010

First published as an Advance Article on the web 16th March 2010

DOI: 10.1039/b924684c

The proton/lithium exchange property of the lithium lanthanum titanate $\text{Li}_{0.30}\text{La}_{0.57}\text{TiO}_3$ (named LLTO) is shown to occur at room temperature under ambient air. The ^1H and ^7Li MAS NMR, TGA analysis and IR spectroscopy techniques are used to probe reaction mechanisms. XRPD analysis gives evidence of the topotactic character of this exchange reaction. As for exchange in aqueous solution, it is shown that $\text{Li}_{0.30}\text{La}_{0.57}\text{TiO}_3$ is able to dissociate water on the grain surface and then to exchange H^+ for Li^+ into the perovskite structure. Lithium hydroxide is then formed on the grain surface and afterwards reacts with CO_2 contained in air to form Li_2CO_3 . It is shown that this mechanism is reversible. When the aged sample (aging in air for 5 months at room temperature) is annealed at $400\text{ }^\circ\text{C}$ for two hours, the initial LLTO sample is totally recovered, a mass loss is observed and the carbonate signal in IR spectra disappears, demonstrating the reversibility of the carbonation reaction process.

Introduction

The titanium-based perovskite phases $(\text{Li}_{3x}\text{La}_{2/3-x}\square_{1/3-2x})\text{TiO}_3$, hereafter named LLTO, have attracted much attention since the papers of Belous *et al.* in 1987¹ and Inaguma *et al.* in 1993² who reported a bulk lithium conductivity as high as 10^{-3} S cm^{-1} at room temperature, for $x = 0.10$. This is one of the highest ionic conductivity in crystalline lithium-ion conductors reported at the time.³ Ion migration occurs through the conduction paths formed by Li^+ ions and vacancies \square , present in the A-sites of the ABO_3 perovskite structure. Structural data have been published by Fourquet *et al.*⁴ and Robertson *et al.*⁵ These authors agree to say that a pure solid solution exists in the composition range $0.04 < x < 0.14$. These phases $(\text{Li}_{3x}\text{La}_{2/3-x}\square_{1/3-2x})\text{TiO}_3$ can be exchanged in nitric acid,⁶ but also in water⁷ with the same efficiency. The ionic exchange reaction in water performed on $\text{Li}_{0.3}\text{La}_{0.57}\text{TiO}_3$ leads to the formation of the protonated phase $\text{H}_{0.25}\text{Li}_{0.05}\text{La}_{0.57}\text{TiO}_3$, demonstrating the affinity of this material for water.

It is known from the literature that lithium containing materials can be used for CO_2 retention. In this context, it has been shown that lithium hydroxide, which is a hygroscopic compound, can be used in its monohydrated form for retention of CO_2 with high efficiency.^{8,9} The chemical sorption of CO_2 can also occur on lithium oxide, efficiency as high as 86 mol% conversion of Li_2O to Li_2CO_3 is reported by Mosqueda *et al.* after heating at $600\text{ }^\circ\text{C}$ for 2 h.¹⁰ Some lithium ceramics, such as lithium zirconates,^{11–14} lithium silicates¹⁵ and lithium titanates¹⁶ can also

show CO_2 sorption. All these ceramics react with CO_2 at high temperature, *i.e.* above $450\text{ }^\circ\text{C}$ for zirconates, above $650\text{ }^\circ\text{C}$ for silicates and above $850\text{ }^\circ\text{C}$ for titanates.

The effect of CO_2 on cathode materials used for secondary lithium batteries has been also extensively investigated. Indeed, a chemical instability of the cathodes has been shown during storage in air. In particular, the reaction of CO_2 with cathode materials generally leads to a reduction of the batteries performances. In the case of $\text{Li}_{1+z}\text{Ni}_{1-x-y}\text{Co}_x\text{M}_y\text{O}_2$ ($\text{M} = \text{Al}, \text{Mn}$), it has been shown that Li_2O is present on the sample surface and is able to react with CO_2 in air to produce Li_2CO_3 .¹⁷ But carbon dioxide can also produce lithium deintercalation and lithium carbonate formation, as in $\text{LiNi}_{0.81}\text{Co}_{0.16}\text{Al}_{0.03}\text{O}_2$.^{18,19} This reaction can occur at room temperature with a conversion of 8% after 500 h in air at 55% RH. This conversion can reach up to 70% under atmospheric CO_2 at $675\text{ }^\circ\text{C}$. Ménétrier *et al.* have suggested that the deintercalation of lithium ions is accompanied with an intercalation of protons, proving that an ionic exchange reaction occurs upon hydration of $\text{Li}(\text{Ni}_{1-y-z})\text{Co}_y\text{Al}_z\text{O}_2$ sample.²⁰

In a recent paper, Simon *et al.* showed that lithium titanate, $\text{Li}_4\text{Ti}_5\text{O}_{12}$, can be exchanged in acid solution.²¹ Electrochemical tests indicate that Li^+ ions are intercalated then deintercalated from the material and a sample exposed to air more than 6 months also exhibits potential curves which characterize a Li^+/H^+ exchange. After annealing at $900\text{ }^\circ\text{C}$, the received commercial sample feature was recovered. A suspected behavior with air was suggested and care in storage was therefore advised.

In this study, it will be shown that an ionic exchange occurs in ambient air at room temperature in $\text{Li}_{0.3}\text{La}_{0.57}\text{TiO}_3$ sample. A mechanism is proposed to explain the aging reaction process. An intermediate protonated phase reacts with carbon dioxide from air leading to the formation of lithium carbonate Li_2CO_3 . To highlight the aging reaction process, X-Ray Powder Diffraction (XRPD) analysis was used to show that a topotactic exchange reaction occurs. Differential thermal analysis (DTA) was performed and

^aLaboratoire de Physique de l'Etat Condensé (UMR 6087 CNRS), Institut de Recherche en Ingénierie Moléculaire et Matériaux Fonctionnels (FR 2575 CNRS), Université du Maine, Avenue O. Messiaen, 72085, Le Mans Cedex 9, France

^bLaboratoire des Oxydes et Fluorures (UMR 6010 CNRS), Institut de Recherche en Ingénierie Moléculaire et Matériaux Fonctionnels (FR 2575 CNRS), Université du Maine, Avenue O. Messiaen, 72085, Le Mans Cedex 9, France. E-mail: odile.bohnke@univ-lemans.fr; Fax: 33-2-43 83 35 06; Tel: 33-2-43 83 33 54

Thermogravimetric Analysis (TGA) measurements enabled the mass loss to be quantified. Infra Red (IR) spectroscopy revealed the presence of carbonate whereas the properties of the hydrogen and lithium nucleus are illustrated using ^1H and ^7Li Magic Angle Spinning Nuclear Magnetic Resonance (MAS NMR).

Experimental

$\text{Li}_{0.3}\text{La}_{0.57}\text{TiO}_3$ samples were analyzed after synthesis (the corresponding sample is named “AS” in the following), and after an aging process in air at room temperature ($\sim 20^\circ\text{C}$) for 5 months (named “AGED”). The aged sample was further annealed at 400°C in air for two hours to form the sample named “OA”.

Preparation of LLTO powder

The lithium lanthanum titanate, $\text{Li}_{0.30}\text{La}_{0.57}\text{TiO}_3$, was prepared by the Pechini method.²² The synthesis procedure was described in ref. 23. The titanate powder was obtained after a thermal treatment of the precursor powder at 900°C in air. A pellet of this powder was sintered at 1000°C in air for two hours. After sintering, the pellet was ground in an agate mortar to obtain the powder studied in this work. All samples (AS, AGED, OA) came from the same synthesis. The aging of the samples has been performed in air at room temperature under a relative humidity close to 50%.

Characterization of the powder

XRPD, TGA, IR spectroscopy and MAS NMR techniques were used to characterize the samples. XRPD patterns were collected at room temperature with a Philips X'Pert PRO diffractometer (Cu-K α radiation) in the 2θ range from 8 to 134.2° with an increment step of 0.0167° and a data acquisition of 7 h 33 min. XRPD patterns were analyzed by the Rietveld method²⁴ using the FULLPROF software.²⁵

IR spectra were obtained with a FTIR spectrometer (Nicolet AVATAR 370 DTGS) in the spectral range from 400 to 4000 cm^{-1} with a resolution of 2 cm^{-1} . The sample consisted of pellets prepared by pressing a mechanically homogenized mixture of LLTO powder with dehydrated KBr (1 wt%).

TGA of LLTO powder was carried out using a TA Instruments SDT 2960 system, with a heating rate of 5°C min^{-1} in the temperature range from 25 to 1000°C under a flowing air atmosphere. A Pt crucible was used.

NMR spectra were recorded with a Bruker Avance 300 spectrometer working at a frequency $\nu_0 = 116.64\text{ MHz}$ for ^7Li and $\nu_0 = 300.13\text{ MHz}$ for ^1H . The experiments were performed on powdered samples spinning at the magic angle with a standard 4 mm MAS probe. ^7Li spectra were referenced from LiCl saturated solution, and the proton ones were referenced from TMS (tetramethylsilane). The $\pi/2$ pulse duration was $4\text{ }\mu\text{s}$ for both nuclei. This pulse duration was sufficient to obtain a non selective spectrum in the case of quadrupolar ^7Li nucleus. For the ^1H nucleus, the recycle time was 200 s and 32 scans were accumulated. For ^7Li nucleus, the recycle time was 2000 s and 8 scans were accumulated. Magic Angle Spinning (MAS) one dimension (1D) pulse experiments were performed on ^7Li and ^1H nuclei with frequency rotation $\nu_{\text{R}} = 10\text{ kHz}$. A Hahn echo,^{26–28} with echo delay equal to $10\text{ }\mu\text{s}$, was used for ^1H nucleus. Prior each sequence, a saturation comb is applied. In this paper ^7Li spectra recorded in non synchronized and synchronized modes

and only ^1H spectra recorded in synchronized mode are shown. In the non synchronized mode, the spectral width is 100 kHz and the spinning frequency is 10 kHz . In this case, the spectrum contains both isotropic lines and their spinning side bands. In the synchronized mode, the spectral width equals the rotor spinning frequency (10 kHz) and the spectrum exhibits the isotropic lines only. ^7Li spectrum of commercial Li_2CO_3 (Aldrich, 99.997%) was also recorded. The DMFIT software was used to reconstruct the spectra and obtain the line widths, the peak positions (in Hz or ppm) and the percentage of each contribution.²⁹

Results

The result of the Rietveld refinement for the AS sample is presented in Fig. 1a. All the peaks in the diffraction pattern can be unambiguously indexed in a tetragonal unit cell (space group $P4/mmm$). As suggested by Fourquet *et al.*,⁴ the reflections were divided into two sets of lines and the “two phases” option of FULLPROF software was used in the refinement. One set is formed of (hkl) reflections with $l = 2n$ while superstructure peaks with $l = 2n+1$ are included in the second set. The same structural model is applied to both “phases”. The lanthanum content was refined between the two possible crystallographic sites (1a) (0,0,0) and (1b) (0,0,1/2) but constrained to give a total number of lanthanum atoms consistent with the $x = 0.10$ value.

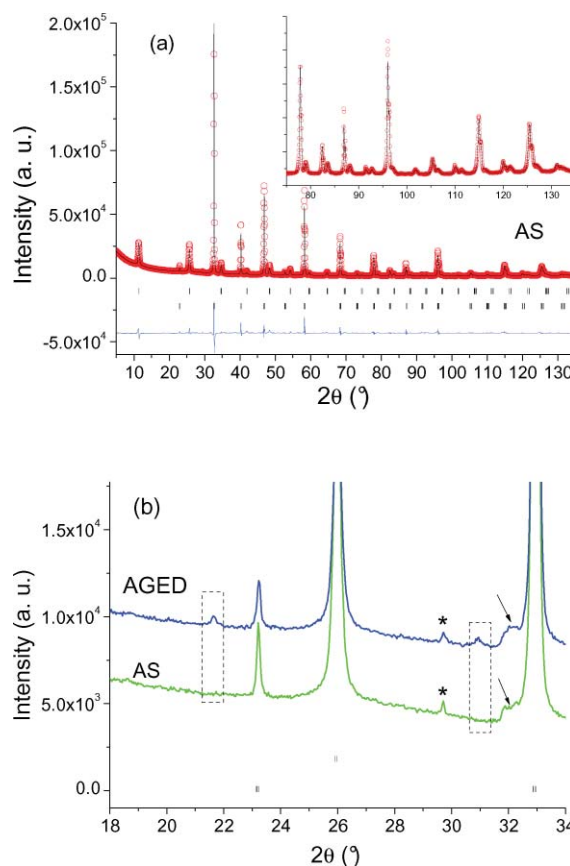


Fig. 1 Observed, calculated and difference profiles of the final Rietveld refinement for AS sample. Inset is a zoom of the 2θ range from 75 to 134.2° . (b) Comparison of XRPD patterns for AS and AGED samples in the 2θ range from 18 to 34° . The arrows indicate the filter apparatus effect.

Table 1 Unit cell parameters and reliability factors obtained after Rietveld refinement of XRPD patterns of the AS and AGED samples

	$a = b/\text{\AA}$	$c/\text{\AA}$	$R_1 (l = 2n)$	$R_1 (l = 2n + 1)$	R_p	R_{wp}	R_{exp}
AS	3.87335(3)	7.76258(6)	11.2	4.1	12.6	12.3	3.2
AGED	3.87335(3)	7.76604(8)	7.5	4.9	12	11.3	3.6

The final refinement involved 14 parameters for 194 reflections (98 and 86 in phase 1 ($l = 2n$) and 2 ($l = 2n + 1$) respectively) up to 134.2° . The R -factor values are gathered in Table 1. Results are in good agreement with those obtained in ref. 4.

Fig. 1b shows the XRPD patterns of both AS and AGED samples in the 2θ range from 18 to 34° . The vertical bars “|” on the bottom of the figure indicate the position of the LLTO Bragg peaks. The peak marked with the symbol “*” corresponds to the most intense diffraction peak (102) of LLTO associated with the $K_{\beta 1}$ radiation (1.39222 \AA) of the copper anticathode. These spectra are very similar except in the 21.5° and 31° 2θ regions, shown in the dashed frames. The diffraction lines that appear clearly in the aged sample do not belong to the LLTO structure. However, the lattice constants and atomic coordinates are similar in both AS and AGED samples. As shown in Table 1, all samples have cell parameters with $a = b = a_p$ and $c \approx 2a_p$, where a_p is the cell parameter of the ideal perovskite structure.

TG curves measured in the temperature range from 25°C to 1000°C on AS and AGED samples of LLTO powders are shown in Fig. 2. After synthesis, it is shown that the powder is thermally stable in the temperature range investigated since a small weight loss (about 0.4%) is observed between 150 – 300°C . On the other hand, the TG curve obtained on aged powder reveals a larger weight loss between 150°C and 500°C , which accounts for 3.55%, accompanied by an endothermic peak observed on the DTA curve. The amount of adsorbed water on the surface of the powder is small, of the order of 0.02 wt% (not visible in the figure).

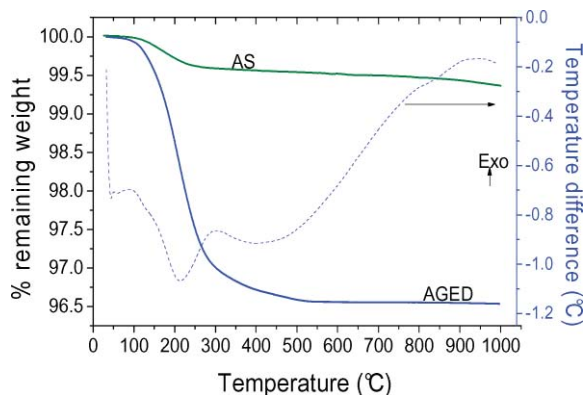


Fig. 2 TG curves in the temperature range from 25°C to 1000°C of the AS and AGED LLTO powder samples. The rise of temperature was $5^\circ \text{C min}^{-1}$. The blue dashed line is for the TD curve for the AGED sample.

Fig. 3 displays IR spectra for AS and AGED LLTO samples recorded in the range from 400 to 4000 cm^{-1} . These spectra are both composed of bands centered at 593 cm^{-1} (related to $\nu_s(\text{Ti-O})$). For the AGED sample, 4 bands (1491 , 1437 , 1088 and 871 cm^{-1}) are straightforwardly attributed to the presence of carbonates. Bands at 1491 and 1437 cm^{-1} are associated with the degeneracy of asymmetric stretching vibration mode ($\nu_{AS}(\text{CO})$).

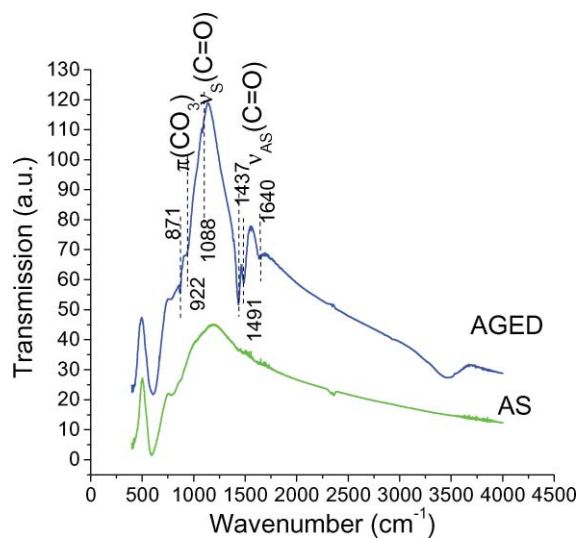


Fig. 3 IR spectra of the AS and AGED LLTO samples recorded in the wavenumber range from 400 to 4000 cm^{-1} .

The $\Delta\nu_3 = 54 \text{ cm}^{-1}$ splitting characterizes a unidentate structure of carbonate.^{30,31} The band at 871 cm^{-1} is related to an out of plane bending (ν_2 , $\pi(\text{CO}_3)$) and the band at 1088 cm^{-1} is assigned to totally symmetric $\nu_s(\text{CO})$.

The bands observed at 1640 and 3460 cm^{-1} are respectively attributed to the bending mode $\delta(\text{H}_2\text{O})$ and the stretching mode $\nu(\text{H}_2\text{O})$. They may be attributed to adsorbed water. However these lines are also observed in the IR spectrum of the LLTO sample exchanged in water,⁷ where protons are inserted in the perovskite structure. In this case, protons are near oxygen atoms, and form $\text{Ti}(\text{OH}_2)$ groups as in titanyl phosphate.³² Then, vibration modes observed are similar to those of adsorbed water. The same observation is done in the $\text{Li}_4\text{Ti}_5\text{O}_{12}$ sample, exchanged in acid solution.²¹ In this case, the insertion of protons results in a vibration at 938 cm^{-1} , due to a lattice coupling of the H^+ -form spinel.^{21,33,34} In the case of H^+ insertion in the perovskite structure, this lattice coupling mode of the proton could explain the vibration at 922 cm^{-1} , observed in AGED LLTO and samples exchanged in water ($\text{Li}_{0.30-y}\text{H}_y$) $\text{La}_{0.57}\text{TiO}_3$.

Fig. 4 shows the superposition of ^7Li MAS NMR spectra for AS and AGED LLTO samples and Li_2CO_3 sample. The AS sample spectrum evidences very small spinning side bands whereas the AGED sample spectrum shows spinning side bands which are strictly identical to those observed for the Li_2CO_3 sample. The inset displays the superposition of isotropic lines of the AGED LLTO sample and Li_2CO_3 , obtained after normalization so as the amplitudes of the spinning side bands of both samples (AGED LLTO and Li_2CO_3) are strictly identical. Then, this inset is a direct view of the relative percentage of Li_2CO_3 in the AGED LLTO sample. The ^7Li MAS NMR spectrum of lithium carbonate is similar to the one obtained by Ménétrier *et al.*²⁰ After aging in air,

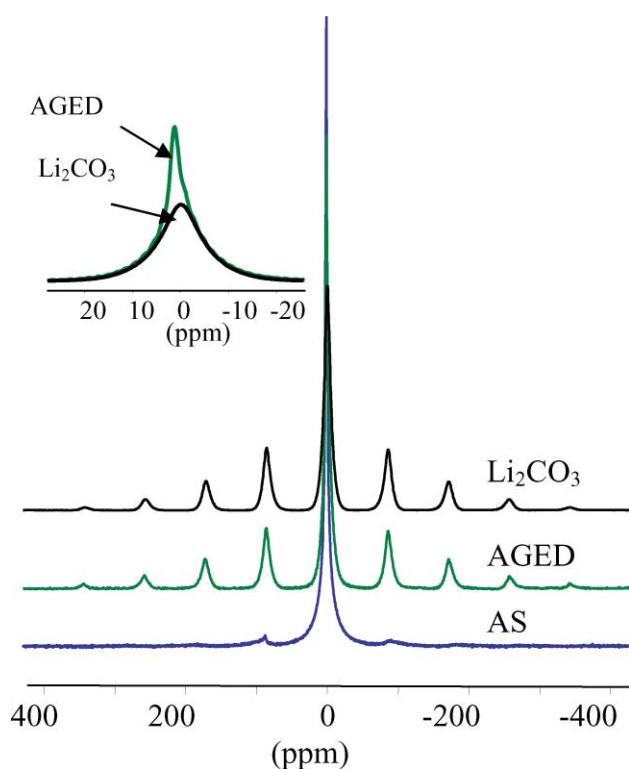


Fig. 4 Superposition of ${}^7\text{Li}$ MAS NMR (10 kHz) spectra (spectral window of 100 kHz) of the AS and AGED LLTO powder samples and of Li_2CO_3 . The inset is the superposition of the isotropic line of Li_2CO_3 and the AGED sample spectra, normalized so that the spinning side bands of both samples are perfectly superposed.

the anisotropy is more significant in the AGED sample than in the AS LLTO one, proving that the lithium environment changes during aging. The fast Li motion in the AS sample averages quadrupolar interaction,³⁵⁻³⁶ whereas in the AGED sample, the averaging process does not act, suggesting that the Li^+ mobility has decreased.

The ${}^7\text{Li}$ synchronized MAS NMR spectra are presented in Fig. 5 and their characteristics are given in Table 2. Fig. 5a displays the superposition of ${}^7\text{Li}$ MAS NMR synchronized spectra of AS and AGED LLTO samples (these spectra have been normalized according to the mass of the powder sample). The spectra of AS and AGED samples are different, the AGED spectrum shows an asymmetric form. The intensity of the line at 1.51 ppm decreases with aging, whereas a new line appears between 0 and -10 ppm. The inset displays the reconstruction of the AS LLTO sample spectrum. The narrow line called Li1 has an isotropic chemical shift of 1.51 ppm and accounts for 51% of the signal intensity. The broad line, at 1.41 ppm, accounts for 49%. These percentages are

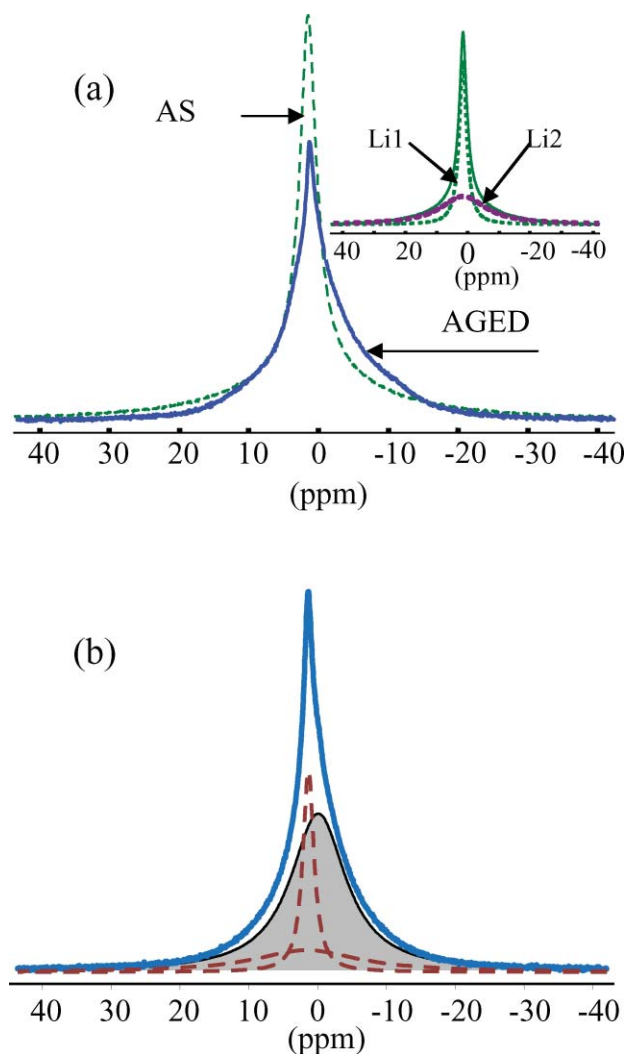


Fig. 5 (a) ${}^7\text{Li}$ MAS NMR 10 kHz spectra (spectral window of 10 kHz) of AS and AGED LLTO powder samples. Spectra have been normalized to the powder mass. The inset shows the reconstruction of the AS sample spectrum. (b) Reconstruction of the AGED sample ${}^7\text{Li}$ NMR spectrum with three lines (grey area is for Li_2CO_3).

in good agreement with those previously determined for samples synthesized by the solid state reaction.³⁵⁻³⁶

The ${}^1\text{H}$ synchronized MAS NMR spectra are shown in Fig. 6. The characteristics of the different line contributions are reported in Table 3. Fig. 6a shows ${}^1\text{H}$ MAS NMR spectra of AS and AGED samples. The intensity of the AGED sample spectrum is about 20 times higher than the AS sample one. The AGED sample spectrum exhibits three lines, (H1, H2 and H3) as shown in the left inset. The right inset shows the reconstruction of the

Table 2 Isotropic chemical shifts δ (ppm), linewidths Δ (ppm) and line intensities (%) of the ${}^7\text{Li}$ NMR spectra for AS, OA, AGED and Li_2CO_3 samples

Line	AS			OA			AGED			Li_2CO_3		
	δ	Δ	%	δ	Δ	%	δ	Δ	%	δ	Δ	%
Li1	1.51	2.83	51	1.49	2.73	49	1.6	1.94	18			
Li2	1.41	17.7	49	1.40	15.8	51	1.61	18.2	16			
Li3							-0.03	9.79	66	-0.03	9.79	100

Table 3 Isotropic chemical shifts δ (ppm), linewidths Δ (ppm) and line intensities (%) of the ^1H NMR lines in AS, AGED and exchanged samples

Line	AS			AGED			Exchange in water [7]		
	δ	Δ	%	δ	Δ	%	δ	Δ	%
H1	9.22	1.96	1.6	8.89	2.35	8.1	8.83	2.61	9.4
H2	5.70	1.62	4.4	6.21	2.04	60.5	6.35	2.08	54.3
H3	3.92	1.2	15.9	3.94	1.37	31.4	3.98	1.83	36.3
H4	4.99	3.2	76.3						

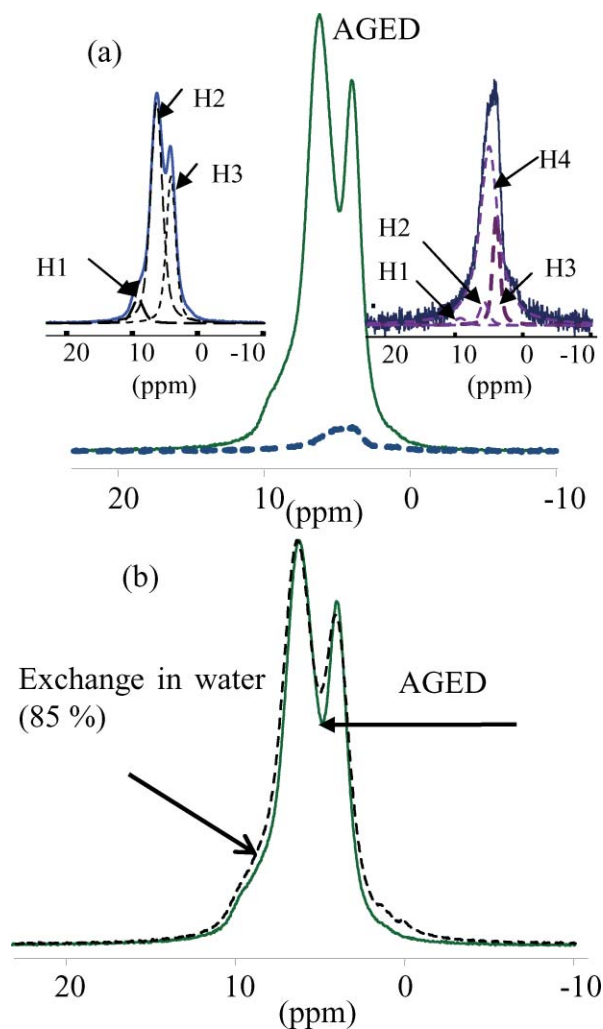


Fig. 6 (a) ^1H MAS NMR (10 kHz) synchronized Hahn Echo spectra recorded on AS (dotted line), and AGED (full line) LLTO powder samples. Left inset shows reconstruction lines (H1, H2 and H3) of AGED curve and right inset is the reconstruction of AS sample and (b) Superposition of ^1H MAS NMR (10 kHz) synchronized Hahn Echo spectra recorded on AGED (full line) LLTO and LLTO synthesized by solid state reaction and exchanged in water (85%) [7].

AS sample spectrum which can be done with four lines. The three lines, H1, H2 and H3 previously observed in the AGED sample, are observed but another predominant line appears, called H4. This line H4 in the AS sample can be attributed to physically adsorbed water.³⁷⁻⁴⁰ As shown in Fig. 6b, the ^1H MAS NMR spectrum of the AGED LLTO is the same as the one obtained for the LLTO

sample synthesized by solid state reaction after exchange (85%) in ultra pure water (black dashed line).⁷

The comparison of IR spectra of AS, AGED and OA samples is illustrated in Fig. 7. After annealing, the lines attributed to carbonate and hydroxyl groups inside the structure or close to the surface disappear and IR spectra of OA and AS samples are then very similar (an annealing at higher temperature than 400 °C will lead to spectra without the Li_2CO_3 lines).

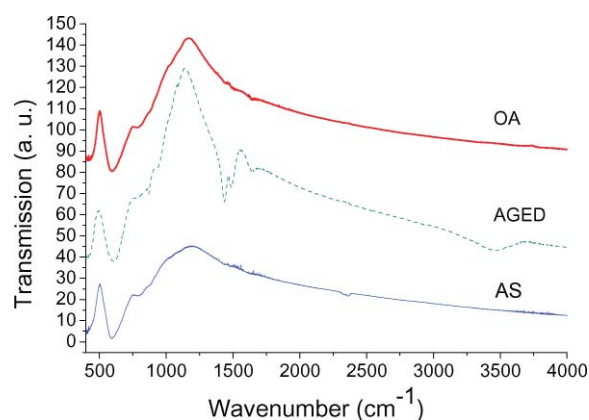


Fig. 7 IR spectra of the AS, AGED and OA LLTO samples in the wavenumber range from 400 to 4000 cm^{-1} .

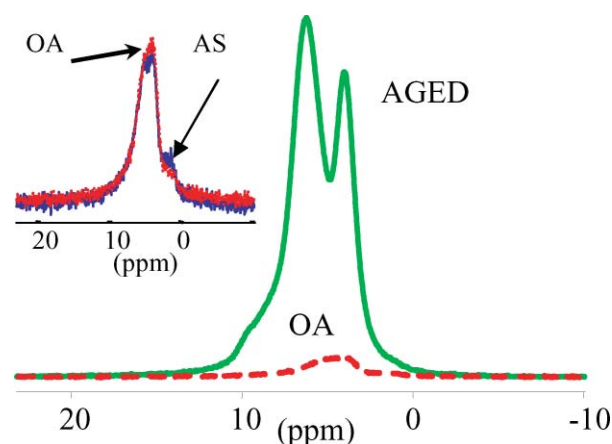


Fig. 8 ^1H MAS NMR (10 kHz) synchronized Hahn Echo spectra recorded on LLTO powder AGED, OA. Inset shows the superposition of ^1H MAS NMR (10 kHz) Hahn Echo spectra of AS and OA samples.

Fig. 8 shows the superposition of ^1H MAS NMR spectra of AGED and OA samples. The intensity of spectra after annealing strongly decreases. As shown in the inset, the weak intensity of ^1H

NMR signal after annealing of the AGED sample is the same as for the sample after synthesis.

Fig. 9a shows the superposition of ^7Li MAS NMR spectra of AS, AGED and OA LLTO samples. After the thermal treatment, the spinning side bands intensity strongly decreases, proving that the particular lithium environment found in AGED sample disappears. This fact is confirmed by the superposition of ^7Li MAS NMR (10 kHz) mass normalized and synchronized spectra of AS, AGED and OA LLTO samples (Fig. 9b). The spectrum of AS and OA samples are identical and both can be reconstructed with two Lorentzian lines, the characteristics of which are given in Table 2. However some residual spinning side bands slightly more intensive than the ones of AS sample are observed. A similar result can also be observed in IR spectra (Fig. 7). All these experiments shown in Fig. 7, 8 and 9 on AS, AGED and OA samples have been performed several times and on several samples. They showed the same characteristics confirming the reproducibility of the observed behavior.⁴¹

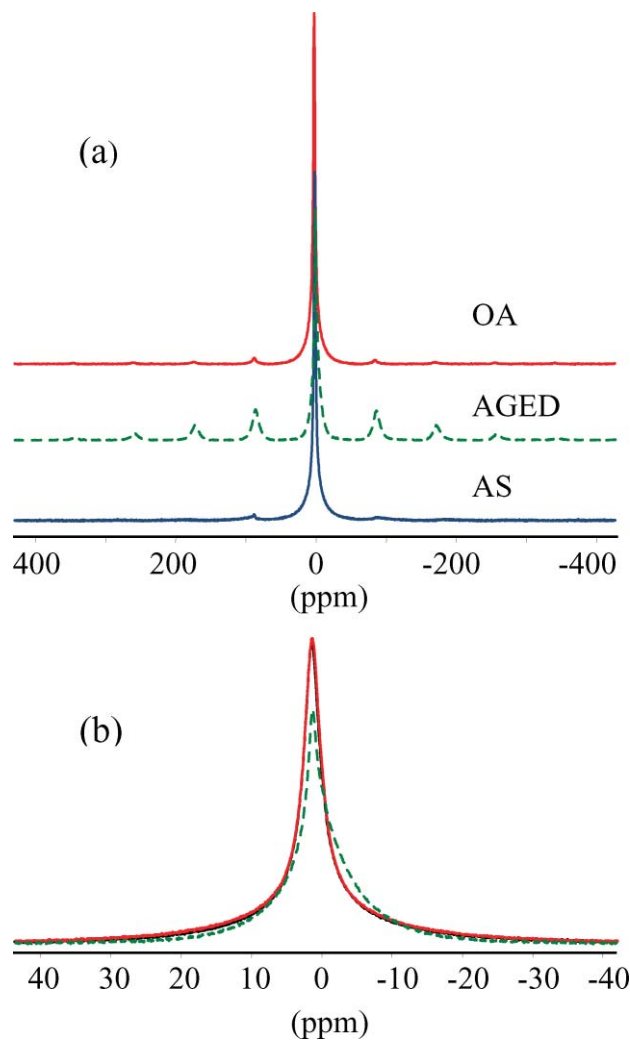
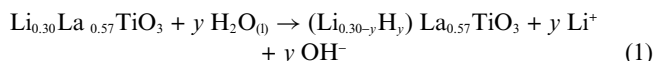


Fig. 9 (a) ^7Li MAS NMR (10 kHz) spectra (spectral window of 100 kHz) of AS, AGED and OA LLTO powder samples. (b) Superposition of ^7Li MAS NMR synchronized (10 kHz) spectra of AS, AGED and OA LLTO powder.

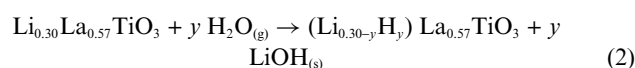
Discussion

^1H MAS NMR of the AGED sample shows clearly the presence of proton sites already observed in the LLTO sample exchanged in water (Fig. 6b). In a previous work,⁷ it has been shown that LLTO can undergo an exchange reaction with water in solution, as follows:



This reaction can be either total when $y = 0.3$ or partial when $y < 0.3$. In the exchanged compound three types of protons were clearly evidenced in the substituted phase. These three protons gave three lines in the ^1H MAS NMR spectrum.⁷

In a first approximation, as proton environments in the AGED sample are identical to the ones exchanged in water, eqn (1) can be rewritten as eqn (2) for reaction with water from air.

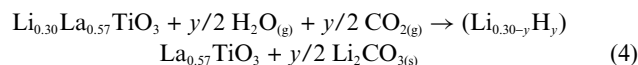


This equation shows the presence of four protons, three protons from the substituted phase and one proton from the lithium hydroxide present on the surface of the titanate after aging. The three former protons are clearly observed in the spectrum of the aged sample but the presence of a fourth proton, which should be in a large amount, is not observed as clearly shown in the left inset of Fig. 6a. This suggests that lithium hydroxide is not the end product of the aging reaction.

The IR analysis performed on the AGED sample gives evidence of the presence of carbonates (Fig. 3). Therefore, when LLTO is in contact with humid air, the compound reacts with water. The exchanged phase is formed, but the LiOH formed on the sample surface reacts with carbon dioxide present in air to form Li_2CO_3 , as described in eqn (3).^{8,9}



Finally, the reaction of the LLTO sample with air can be written as in eqn (4).



This equation explains why only proton sites of the exchanged phase $(\text{Li}_{0.30-y}\text{H}_y)\text{La}_{0.57}\text{TiO}_3$ are present in the ^1H MAS NMR spectrum of the AGED sample. It is worth noting that such a behavior is linked to the high ionic lithium mobility in LLTO.

Therefore our experimental data can be unambiguously explained by the presence of Li_2CO_3 in the AGED sample. The infrared-active vibration modes observed in the IR spectrum at 1491, 1437, 1088 and 871 cm^{-1} can be assigned to the Li_2CO_3 species.⁴²⁻⁴⁴ Further, the diffraction peaks observed in the XRD pattern at 21.3° and 30.6° (Fig. 1b) which appeared only in the AGED sample can be attributed to the Li_2CO_3 intense (1 1 0) and (-2 0 2) diffraction peaks respectively (ICSD data 66941). Finally, the new line that appears in the ^7Li MAS NMR spectrum between 0 and -10 ppm suggests a new Li environment. By keeping constant the position and the width of the line found in the Li_2CO_3 sample (grey area), the AGED sample spectrum can be reconstructed with three lines, as shown in Fig. 5b. The two dashed lines are attributed to the two kinds of lithium present in the LLTO

structure. The relative percentage of the Li_2CO_3 line is then found to be 66%.

Furthermore, the presence of lithium carbonate on the powder of LLTO may explain the difference of the spin–lattice relaxation time T_1 found in the literature.⁴⁵ This shell of carbonate may increase the T_1 value. This result points out the importance of storage of the LLTO powder after synthesis. Further studies are on the way to clarify this point.

It is well known from the literature that carbonation of lithium hydroxide proceeds in a two-step reaction with the formation of the intermediate hydrate ($\text{LiOH}\cdot\text{H}_2\text{O}$) which is a necessary precursor of the CO_2 reaction.^{8,9} A relative humidity between 20 and 70% is required for the reaction to proceed. This is the storage condition of LLTO. After synthesis, adsorbed water is present on the oxide surface and can be detected in the weak intensity ^1H MAS NMR spectrum as the predominant compound (Fig. 6a right inset). Line H4 can then be attributed to this adsorbed water.^{38–41} As carbonation proceeds, water is consumed, the lithium carbonate and the exchanged phase are formed leading to the disappearance of the H4 line and to the increase of the three H1, H2 and H3 lines of $(\text{Li}_{0.30-y}\text{H}_y)\text{La}_{0.57}\text{TiO}_3$ phase in the ^1H MAS NMR spectrum (Fig. 6a left inset).

It is then shown that LLTO reacts at room temperature with water and CO_2 contained in air through a H^+/Li^+ ionic exchange. In a previous work, we already showed that LLTO was unstable in aqueous solutions and that exchange H^+/Li^+ occurs in water with an efficiency of 85% after 24 h at 70 °C. The present study shows that this ionic exchange also occurs in humid air at room temperature. The kinetics are slower than the one in aqueous solution since an efficiency of 66% is found after 5 months of aging. Therefore, the carbonation of LLTO proceeds in a two-step reaction: first the H^+/Li^+ ionic exchange with water and later the reaction with CO_2 from air.

In the literature, other lithium containing ceramics also react with carbon dioxide from the air. But, for lithium zirconate, silicates or titanates^{11–16} the efficiency maximum of the reaction is reached at very high temperature (up to 600 °C), the kinetic is considerably slower at room temperature. The process is described in two steps: First, a fast reaction forming a shell of lithium carbonate on the surface which prevents the lithium reaction with CO_2 from air. Secondly, a slow process of diffusion through Li_2CO_3 occurs and depends strongly on the temperature. For LLTO, we can propose a mechanism for CO_2 and H_2O adsorption (Fig. 10). It illustrates the fact that a shell of lithium carbonate is formed on the surface of the grain with $\text{H}_{0.30}\text{La}_{0.57}\text{TiO}_3$. The interior of the grain would be made of non exchanged LLTO. The lines Li1 and Li2 in the ^7Li MAS NMR spectrum of the AGED LLTO sample are attributed to these non exchanged sites.

It is clearly shown in the IR spectra of Fig. 7 and in the ^1H and ^7Li MAS NMR of Fig. 8 and 9 that the H^+/Li^+ exchange process and the formation of Li_2CO_3 are reversible. After a thermal treatment at 400 °C for two hours, the LLTO sample is recovered. This is confirmed by the mass loss observed during heating of the aged sample above 100 °C (Fig. 2). After annealing, IR spectra do not show evidence of any carbonate signal. ^1H MAS NMR spectrum of sample OA is the same as the one for LLTO after synthesis (inset Fig. 8). The signature of the inserted proton in the perovskite structure disappears. Moreover ^7Li MAS NMR spectra of the OA sample are also similar to the AS sample one, as

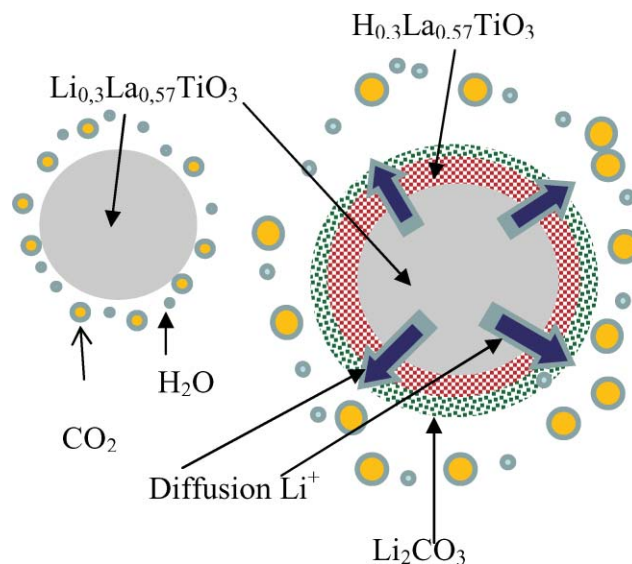
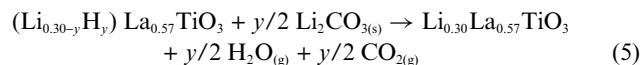


Fig. 10 Scheme of the mechanism proposed for CO_2 and H_2O adsorption on LLTO.

shown in Fig. 9b where the OA sample displays a spectrum without any line between 0 and –10 ppm characteristic of the presence of Li_2CO_3 . The thermal decomposition of $(\text{Li}_{0.30-y}\text{H}_y)\text{La}_{0.57}\text{TiO}_3$ observed in sample exchanged in acid⁶ or water⁷ at 350 °C and the melting point of Li_2CO_3 (710 °C) are not observed, proving that both species react together from 150 °C to 500 °C to form $\text{Li}_{0.30}\text{La}_{0.57}\text{TiO}_3$.

These results demonstrate the reversibility of the carbonation reaction. At 250 °C, the mass loss can be written as in eqn (5).



For a total efficiency ($y = 0.3$) of this reaction, the theoretical mass loss would be equal to 5%. By comparison with the experimental mass loss observed for the AGED sample (3.55%), it can be concluded that the efficiency of the aging process is about 68%. This value can be compared to the value of 66% of Li_2CO_3 previously determined from Fig. 5b. Both similar values show that eqn (4) seems to be very realistic for the reaction of LLTO with CO_2 under humid air at room temperature.

It is the first time, to our knowledge, that ^1H and ^7Li NMR are associated with IR spectroscopy to reveal such a two step behavior in the exchangeable phase LLTO.

Previous work on $\text{Li}_4\text{Ti}_5\text{O}_{12}$ ^{21,46} had already suggested that the exchange process may occur under humid air, but no reaction mechanism was clearly proposed. The Li_2CO_3 formation was explained by the conversion of surface Li_2O with CO_2 .¹⁰ In our study, the efficiency of the process (66%) and ^1H MAS NMR spectra (which is identical to LLTO exchange in water⁷ or acid⁶) is not compatible with exchange only from surface lithium. This is also confirmed by the small value of the specific surface (0.48 $\text{m}^2 \text{g}^{-1}$). Lithium ions which react with carbon dioxide also emerged from the structure because of the high ionic lithium mobility and instability of the lithium containing phase (the protonated phase being thermodynamically more stable).

Conclusions

This work clearly demonstrates that the LLTO powder sample reacts with a humid atmosphere leading to H^+/Li^+ ionic exchange. It proves that this ionic exchange H^+/Li^+ is the first step of the mechanism and occurs with water vapor from air at room temperature. Then, lithium ions emerge from the structure and react with CO_2 from ambient air, to form lithium carbonate and a stable partial protonated phase $(Li_{0.30-y}H_y)La_{0.57}TiO_3$ with the same perovskite structure as sample LLTO. An exchange efficiency of 66% is found after 5 months of aging at room temperature.

The second relevant result is the reversibility of the carbonation reaction. An annealing at 400 °C allows LLTO recovering. This is a very significant result that opens a large avenue of research for all exchangeable phases Li^+/H^+ , to which LLTO belongs.

This study provides an explanation for understanding exchangeable lithium phases. Such samples could be used to retain CO_2 from air to limit the greenhouse effect.

Acknowledgements

The authors would like to thank the laboratory “Unité de Chimie Organique Moléculaire et Macromoléculaire” (UCO2M, UMR CNRS 6011) for access to the IR spectrometer. They would also like to thank Dominique Massiot, Christian Bonhomme and Michel Ménétrier for useful discussions.

References

- 1 A. G. Belous, G. N. Novitskaya, S. V. Polyanetskaya and Y. I. Gornikov, *Zh. Neorg. Khim.*, 1987, **32**, 283.
- 2 Y. Inaguma, L. Chen, M. Itoh, T. Nakamura, T. Uchida, H. Ikuta and M. Wakihara, *Solid State Commun.*, 1993, **86**, 689.
- 3 S. Stramare, V. Thangadurai and W. Weppner, *Chem. Mater.*, 2003, **15**(21), 3974.
- 4 J. L. Fourquet, H. Duroy and M. P. Crosnier-Lopez, *J. Solid State Chem.*, 1996, **127**, 283.
- 5 A. D. Roberston, A. R. West and A. G. Ritchie, *Solid State Ionics*, 1997, **104**, 1.
- 6 N. S. P. Bhuvanesh, O. Bohnké, H. Duroy, M. P. Crosnier-Lopez, J. Emery and J. L. Fourquet, *Mater. Res. Bull.*, 1998, **33**, 1681.
- 7 A. Boulant, P. Maury, J. Emery, J. Y. Buzaré and O. Bohnké, *Chem. Mater.*, 2009, **21**, 2209.
- 8 D. D. Williams and R. R. Miller, *Ind. Eng. Chem. Fundam.*, 1970, **9**, 454.
- 9 D. A. Boryta and A. J. Mass, *Ind. Eng. Chem. Proc. Des. Dev.*, 1971, **10**, 489.
- 10 H. A. Mosqueda, C. Vasquez, P. Bosch and H. Pfeiffer, *Chem. Mater.*, 2006, **18**, 2307.
- 11 A. Iwan, H. Stephenson, W. C. Ketchie and A. A. Lapkin, *Chem. Eng. J.*, 2009, **146**, 249.
- 12 K. Essaki, K. Nakagawa and M. Kato, *J. Ceram. Soc. Japan*, 2001, **109**, 829.
- 13 E. Ochoa-Fernandez, M. Ronning, T. Grande and D. Chen, *Chem. Mater.*, 2006, **18**, 1383.
- 14 H. Pfeiffer, C. Vasquez, V. H. Lara and P. Bosch, *Chem. Mater.*, 2007, **19**, 922.
- 15 C. Gauer and W. Heschel, *J. Mater. Sci.*, 2006, **41**, 2405.
- 16 N. Togashi, T. Okumura and K. Oh-ishi, *J. Ceram. Soc. Jpn.*, 2007, **115**, 324.
- 17 K. Shizuka, C. Kiyohara, K. Shima and Y. Takeda, *J. Power Sources*, 2007, **166**, 233.
- 18 K. Matsumoto, R. Kuzuo, K. Takeya and A. Yamanaka, *J. Power Sources*, 1999, **81–82**, 558.
- 19 G. V. Zhuang, G. Chen, J. Shim, X. Song, P. N. Ross and J. T. Richardson, *J. Power Sources*, 2004, **134**, 293.
- 20 M. Ménétrier, C. Vaysse, L. Croguennec, C. Delmas, C. Jordy, F. Bonhomme and P. Biensan, *Electrochem. Solid-State Lett.*, 2004, **7**, A140–A143.
- 21 D. R. Simon, E. M. Kelder, M. Wagemaker, F. M. Mulder and J. Schoonman, *Solid State Ionics*, 2006, **177**, 2759.
- 22 *U. S. Pat.* 3,330,397, 1967.
- 23 M. Vijayakumar, Y. Inaguma, W. Mashiko, M. P. Crosnier-Lopez and C. Bohnké, *Chem. Mater.*, 2004, **16**, 2719.
- 24 H. M. Rietveld, *J. Appl. Crystallogr.*, 1969, **2**, 65.
- 25 J. Rodriguez-Carvajal, *FULLPROF program: Rietveld Pattern Matching Analysis of Powder Patterns*, ILL, Grenoble, 1990.
- 26 E. L. Hahn, *Phys. Rev.*, 1950, **80**, 580.
- 27 J. Lowe, *Bull. Am. Phys. Soc.*, 1957, **2**, 344.
- 28 S. R. Hartmann and E. L. Hahn, *Phys. Rev.*, 1962, **128**, 2042.
- 29 D. Massiot, F. Fayon, M. Capron, I. King, S. Le Calvé, B. Alonso, J. O. Durand, B. Bujoli, Z. Gan and G. Hoaston, *Magn. Reson. Chem.*, 2002, **40**, 70.
- 30 G. Busca and V. Lorenzelli, *Mater. Chem.*, 1982, **7**, 89.
- 31 J. C. Lavalley, *Catal. Today*, 1996, **27**, 377.
- 32 S. Benmokhtar, A. El jazouli, J. P. Chaminade, P. Gravereau, M. Ménétrier and F. Bourée, *J. Solid State Chem.*, 2007, **180**, 2713.
- 33 P. Lavela, L. Sanchez, J. L. Tirado, S. Bach and J. P. Pereira-Ramos, *J. Solid State Chem.*, 2000, **150**, 196.
- 34 P. Aitchison, B. Ammundsen, T. Bell, D. Jones, J. Rozière, G. Burns, H. Berg, R. Tellgren and J. Thomas, *J. Phys. B*, 2000, **276–278**, 847.
- 35 J. Emery, O. Bohnké, J. L. Fourquet, J. Y. Buzaré, P. Florian and D. Massiot, *C.R. Chimie*, 2001, **4**, 845.
- 36 J. Emery, O. Bohnké, J. L. Fourquet, J. Y. Buzaré, P. Florian and D. Massiot, *J. Phys.: Condens. Matter*, 2002, **14**, 523.
- 37 M. Jalbring, D. E. Sandström, O. N. Antzutkin and W. Forsling, *Langmuir*, 2006, **22**, 11060.
- 38 Y. A. Nosaka, T. Fujiwara, H. Yagi, H. Akutsu and Y. Nosaka, *Langmuir*, 2003, **19**, 1935.
- 39 G. Scholz, I. Dörfel, D. Heidemann, M. Feist and R. Stösser, *J. Solid State Chem.*, 2006, **179**, 1119.
- 40 J. Soria, J. Sanz, I. Sobrados, J. M. Coronado, F. Fresno and M. D. Hernandez-Alonso, *Catal. Today*, 2007, **129**, 240.
- 41 A. Boulant, PhD Dissertation, Université du Maine, Le Mans (2009).
- 42 P. Pasierb, S. Komornicki, M. Rokita and M. Rekas, *J. Mol. Struct.*, 2001, **596**, 151.
- 43 K. Buijs and C. J. H. Schutte, *Spectrochim. Acta*, 1961, **17**, 927.
- 44 M. H. Brooker and J. B. Bates, *J. Chem. Phys.*, 1971, **54**, 4788.
- 45 Y. Hirakoso, Y. Harada, J. Kuwano, Y. Saito, Y. Ishikawa and T. Eguchi, *Key Eng. Mater.*, 1999, **169–170**, 209.
- 46 M. Q. Snyder, W. J. DeSisto and C. P. Tripp, *Appl. Surf. Sci.*, 2007, **253**, 9336.